Reconstructing 6-hourly PM$_{2.5}$ datasets from 1960 to 2020 in China

Junting Zhong[1], Xiaoye Zhang[1, 4*], Ke Gui[1], Jie Liao[2], Ye Fei[2], Lipeng Jiang[3], Lifeng Guo[1], Liangke Liu[5], Huizheng Che[1], Yaqiang Wang[1], Deying Wang[1], Zijiang Zhou[2]

[1]State Key Laboratory of Severe Weather & Key Laboratory of Atmospheric Chemistry of CMA, Chinese Academy of Meteorological Sciences, Beijing, 100081, China

[2] National Meteorological Information Center, Beijing, 100081, China

[3] Earth System Numerical Prediction Center, Beijing, 100081, China

[4]Center for Excellence in Regional Atmospheric Environment, IUE, Chinese Academy of Sciences, Xiamen, 361021, China.

[5]Department of Earth System Science, Tsinghua University, Beijing 100084, China

Correspondence to: Xiaoye Zhang (xiaoye@cma.gov.cn)

Abstract

Fine particulate matter ($PM_{2.5}$) has altered radiation balance on earth and raised environmental and health risks for decades, but only been monitored widely since 2013 in China. Historical long-term $PM_{2.5}$ records with high temporal resolution are essential but lacking for both research and environmental management. Here, we reconstruct a site-based $PM_{2.5}$ dataset at 6-hour intervals from 1960 to 2020 that combines long-term visibility, conventional meteorological observations, emissions, and elevation. The $PM_{2.5}$ concentration at each site is estimated based on an advanced machine learning model, LightGBM, that takes advantage of spatial features from 20 surrounding meteorological stations. Our model's performance is comparable or even better than those of previous studies in by-year cross validation (CV) ($R^2=0.7$) and spatial CV ($R^2=0.76$), and more advantageous in long-term records and high temporal resolution. This model also reconstructs a 0.25°×0.25°, 6-hourly, gridded $PM_{2.5}$ dataset by incorporating spatial features. The results show $PM_{2.5}$ pollution worsens gradually or maintains before 2010 from an interdecadal scale but mitigates in the following decade. Although the turning points vary in different regions, $PM_{2.5}$ mass concentrations in key regions decreased significantly after 2013 due to clean air actions. In particular, the annual average value of $PM_{2.5}$ in 2020 is nearly at the lowest value in history since 1960. These two $PM_{2.5}$ datasets (publicly available at https://doi.org/10.5281/zenodo.6372847) provide spatiotemporal variations at high resolution, which lay the foundation of research studies associated with air pollution, climate change, and atmospheric chemical reanalysis.

1 Introduction

In the past decades, anthropogenic emissions of reactive gases and aerosols have been emitted increasingly in the atmosphere and thus led to a substantial increase in fine particulate matter ($PM_{2.5}$). Increased $PM_{2.5}$ has strongly interacted with solar radiation through absorption and scattering, thereby reducing visibility and influencing the earth's radiance balance. Inhalable $PM_{2.5}$ has increased human morbidity and mortality through penetrating the respiratory system (Pope et al., 2002; Beelen et al., 2007; Chen et al., 2016b). To evaluate the impacts of $PM_{2.5}$ pollution on environment, climate, and health, the primary concern is to understand the spatiotemporal variations of $PM_{2.5}$ concentrations. Namely, extended $PM_{2.5}$ records with high temporal resolution lay the foundation of research studies associated with air pollution, climate change, and environmental health. Nevertheless, it was not until 2013 that the Ministry of Ecology and Environment (MEE) established a nationwide $PM_{2.5}$ monitoring network. Long-term, accurate historical $PM_{2.5}$ datasets are lacking for both research and environmental management.

Chemical transport models (CTMs) are expected to simulate the spatial and temporal variations of $PM_{2.5}$ with reasonable emission inventories inputted. However, significant uncertainties still exist in historical emission inventories and physicochemical mechanisms, which resulted in inevitable biases in the simulated absolute values of $PM_{2.5}$. Satellite-based aerosol optical depth (AOD), which measures the aerosol extinction of the solar beam, is an indicator of ground-level aerosols. AOD data products from Moderate Resolution Imaging Spectroradiometer (MODIS) have broad spatial coverage and relatively long observation periods (~ 20 years). Therefore, assimilating satellite-retrieved AOD to construct atmospheric chemical reanalysis is a practical approach to reduce $PM_{2.5}$ biases. In recent years, several international aerosol reanalysis datasets have been developed preliminarily, including the reanalysis data produced by the Copernicus Atmosphere Monitoring Service (CAMS) from the European Centre for Medium-Range Weather Forecasts (ECMWF) (Inness et al., 2019), the Modern-Era Retrospective analysis for Research and Applications, Version 2 (MERRA-2) from the National Aeronautics and Space Administration (NASA) (Gelaro et al., 2017; Randles et al., 2017), aerosol reanalysis from the Navy Aerosol Analysis and Prediction System (NAAPS) (Lynch et al., 2016) and the Japanese Reanalysis for Aerosol (JRAero) from the Japanese Meteorological Agency (Yumimoto et al., 2017). In particular, CAMS produced gridded PM_1, $PM_{2.5,}$ and PM_{10} data at 80 km resolution since 2003 by assimilating satellite retrievals of total AOD, total tropospheric NO_2 column, total O_3 column, CO column, and vertical profiles (Inness et al., 2019). MERRA-2 reanalysis includes $PM_{2.5}$ and PM_{10} at 50 km resolution since 1980 by assimilating ground-based and satellite-retrieval (Gelaro et al., 2017; Randles et al., 2017). NAAPS generates gridded AOD data at ~100 km resolution from 2003 to 2013 by assimilating satellite-based AOD products (Lynch et al., 2016). JRAero provides $PM_{2.5}$ and PM_{10} at ~100 km resolution from 2011 to 2015 by assimilating satellite AOD data (Yumimoto et al., 2017). These reanalysis data have contributed significantly to research in aerosol-related fields. However, there are still some weaknesses in accuracy, spatial resolution, time span, and types of assimilated data. In China, the highest horizontal resolution of the four reanalysis is only 50 km, and this coarse grid setting may not be sufficient to capture the spatial differences in atmospheric pollutants at regional scales. In terms of the type of aerosol data assimilation, these reanalysis data mainly assimilate satellite-based and ground-based AOD, and do not take into account ground $PM_{2.5}$ observations.

To overcome the reanalysis's weaknesses in low spatial resolution and high biases, numerical

79   researchers focus on constructing relatively long-term PM$_{2.5}$ datasets based on machine learning
80   techniques that fuse multisource data, including satellite-retrieved AOD, CTM simulations, and
81   even atmospheric chemical reanalysis. For example, Ma et al. (2016) estimated daily PM$_{2.5}$ records
82   at 0.1° resolution between 2004-2013 with MODIS AOD. Liang et al. (2020) rebuilt monthly PM$_{2.5}$
83   concentrations at 1 km resolution during 2000-2016 based on the multiangle implementation of
84   atmospheric correction (MAIAC) from MODIS and reanalysis AOD and PM$_{2.5}$ data from MERRA-
85   2. Geng et al. (2021) reconstructed daily, 10 km PM$_{2.5}$ data between 2000-2020 with MODIS AOD
86   and CTM simulations. Wei et al. (2021) regenerated monthly, 1 km PM$_{2.5}$ records between 2000-
87   2018 based on MAIAC AOD. Huang et al. (2021) estimated 1 km × 1 km PM$_{2.5}$ concentrations daily
88   between 2013-2019 based on MAIAC AOD and CTM outputs. However, some inherent limitations
89   in satellited-based AOD are challenging to overcome. Due to the low sampling frequency of
90   satellite-retrieved AOD, AOD-based PM$_{2.5}$ datasets are limited to a maximum temporal resolution
91   of one day. With AOD over land unavailable before 2000, these PM$_{2.5}$ datasets can only be back-
92   calculated to 2000 at the earliest.

93   Compared with satellite data, ground-based meteorological observations have the advantages
94   of long sequence time, high temporal resolution, and good data integrity. In China, the national
95   meteorological observation network of the China Meteorological Administration (CMA) was
96   established in the 1950s and is capable of continuously observing 6-hourly meteorological data on
97   visibility and conventional meteorological variables, including temperature, pressure, wind, and
98   humidity. The number of national stations exceeded 2,000 in 1960 and has stabilized at around 2,450
99   afterward. Therefore, better results may be achieved if these ground-based meteorological data can
100 be used to estimate historical PM$_{2.5}$ data in China. Liu et al. (2017) first estimated monthly visibility-
101 based PM$_{2.5}$ concentrations between 1957-1964 and 1973-2014 based on 674 publicly available
102 meteorological stations. Gui et al. (2020) constructed a virtual daily PM$_{2.5}$ network at 1180
103 meteorological sites between 2017-2018. Our previous research also shows that the visibility-based
104 machine learning model that takes advantage of spatial features has great potential in reconstructing
105 historical PM$_{2.5}$ datasets with long-term records and high temporal resolution (Zhong et al., 2021).
106 In this study, we reconstruct a site-based PM$_{2.5}$ dataset at 6-hour intervals from 1960 to 2020 based
107 on long-term visibility and conventional meteorological observations from ~2450 national stations,
108 together with emissions and elevation. The PM$_{2.5}$ concentration at each site is estimated based on a
109 Light Gradient Boosting Machine (LightGBM) model that takes advantage of spatial features from
110 20 surrounding meteorological stations. By incorporating spatial features, this model also
111 reconstructs a 0.25°×0.25°, 6-hourly, gridded PM$_{2.5}$ dataset. These two PM$_{2.5}$ datasets provide
112 spatiotemporal variations at high resolution, which constitute the basis for research studies
113 associated with air pollution, climate change, and atmospheric chemical reanalysis.

114

2 Data and Methods

2.1 Multisource input data

Observational PM$_{2.5}$ data. The MEE began laying out a PM$_{2.5}$ monitoring network in January 2013, expanding the scope from key regions including the North China Plain (NCP), the Yangtze River Delta (YRD) ,the   Pearl River Delta (PRD), and the Sichuan Basin (SB) as well as municipalities directly under the Central Government and provincial capitals, to 113 key and model cities for environmental protection, and eventually to all cities above prefecture level, with the number of observation sites expanded from the initial 520 to over 1,600. Since then, PM$_{2.5}$ mass concentrations have been recorded continuously using the β-absorption methods or a micro-oscillating balance following a standard protocol (Huang et al., 2021). Hourly PM$_{2.5}$ data of all sites between 2013-2020 are collected from the China National Environmental Monitoring Center (CNEMC, http://www.cnemc.cn). To produce high-quality PM$_{2.5}$ data, a series of quality controls were conducted, including integrity checking, duplicate rejection, and outlier handling. All sites with the proportion of valid PM$_{2.5}$ records exceeding 60% were considered. For each site, identical data for 3 consecutive hours were excluded first, and PM$_{2.5}$ values over three standard deviations from 24-hour and 3-day moving average were regarded as outliers and discarded then. Eventually, PM$_{2.5}$ data from 1485 sites remained for model development and application. In addition, pre-2013 PM$_{2.5}$ measurements in US embassies in Beijing and Shanghai are used for independent validation evaluations (http://www.stateair.net/web/historical).

Visibility and conventional meteorological data. The CMA established a national meteorological observation network in the 1950s, with the station number exceeding 2000 at the beginning and stabilizing at ~2,450 afterward. The observation network can continuously record meteorological data on visibility and conventional meteorological variables, including temperature, pressure, wind, and humidity. In recent years, meteorological observations, including 6-hourly records between 1960-2020 and hourly records, have been collected from the National Meteorological Information Center (NMIC). Due to the inconsistency of visibility data in terms of observation methods, we conducted a series of data conversions to ensure continuous and consistent data. Visibility data recorded on a scale ranging from 0 to 9 between 1960-1979 were converted to numerical data based on probability density distributions. Specifically, the probability density distribution of visibility for each of the ten years before and after 1980 was calculated at first. The numerical visibility from 1980 to 1989 was graded into classes, with the median value of each class being the corresponding value for each station, and finally, the class observations were converted into numerical observations. From September 2013 to 2016, visibility measurements gradually shifted from 6-hourly manual observations to 1-hourly automatic observations site-by-site. In keeping with manual measurements, the automatic records, which are slighter lower than manual measurements, were calibrated by dividing 0.75 following the guideline from the CMA (Cma, 2014).

Emission inventories and elevation. Historical anthropogenic emissions from 1960-2012 are taken from Peking global emission inventories, developed using a bottom-up approach with spatial resolution at 0.1°×0.1° and temporal resolution at 1-month intervals (http://inventory.pku.edu.cn) (Chen et al., 2016a; Huang et al., 2014; Huang et al., 2015; Wang et al., 2014). Current anthropogenic emissions during 2013-2020 are from the multiresolution Emission Inventory in

156   China (MEIC, http://meicmodel.org) (Zhang et al., 2009; Zheng et al., 2018; Zheng et al., 2021).
157   Six emission variables from these two inventories are used as inputs for model development,
158   including $PM_{2.5}$, NO_x, SO_2, NH_3, BC, OC, and CO. Thirty-meter elevation data are collected from
159   the Global Digital Elevation Model (GDEM) version 2 (https://earthexplorer.usgs.gov). Both
160   emission and elevation data are interpolated from grids to sites to match existing $PM_{2.5}$ sites.

161   *Auxiliary data*. Monthly Normalized Difference Vegetation Index (NDVI) products are
162   downloaded from Level-1 and Atmosphere Archive & Distribution System Distributed Active
163   Archive Center (LADDS DAAC, https://ladsweb.modaps.eosdis.nasa.gov). Land cover
164   classification data are taken from National Geographic Information Resources Catalogue Service
165   System (https://www.webmap.cn/mapDataAction.do?method=globalLandCover). Population data
166   are taken from the Gridded Population of the World version 4 (GPWv4,
167   https://sedac.ciesin.columbia.edu/data/collection/gpw-v4) and are calibrated based on the total
168   population in China City Yearbooks. NDVI, Land cover, and population data are also interpolated
169   according to $PM_{2.5}$ sites and trained as inputs for model development. However, during the model
170   training process, we found that these data had little or no improvement in the hindcast capability of
171   the model, and the time span of these data is insufficient for long-term historical retrieval. Hence,
172   these auxiliary data are not used in model building.

2.2 Spatiotemporal feature extraction

174   For each $PM_{2.5}$ site, we extract five variables as temporal inputs, including year, month, day,
175   hour, and day of year. The longitude and latitude variables are taken out as location inputs (Fig. 1b).
176   Visibility, RH, and temperature from the nearest meteorological station of each $PM_{2.5}$ are used as
177   basic meteorological inputs. The distance between these two sites was also added as a feature. In
178   addition to the influence of the nearest meteorological station, $PM_{2.5}$ concentrations at a site are also
179   affected by surrounding conditions. For example, transport of pollution due to air movement is the
180   main cause for the early stage of heavy pollution episodes (Zhong et al., 2017; Zhong et al., 2018).
181   Hence, we need to consider spatial effects from surrounding meteorological stations. Our previous
182   study developed a novel feature engineering approach, which incorporated surrounding impact by
183   extracting spatial features (Zhong et al., 2021). Specifically, the remaining 19 nearest stations were
184   matched for each $PM_{2.5}$ site, except the nearest meteorological station. Five variables, including
185   longitude, latitude, temperature, visibility, and RH, were selected from the 19 stations. Then, we
186   calculated the maximum, the minimum, the average value, the skewness value, and the standard
187   deviation for each of the five variables. These produced features, which take advantage of
188   surrounding conditions, are also considered as inputs. After spatiotemporal feature extraction, a total
189   of 71 features were used as inputs for model training. To reduce computation and training time with
190   guaranteed accuracy, the top 35 features in order of importance during small-sample-testing
191   processes are used for the following model training and hindcasting. These features included
192   visibility, temporal features, spatial features, emission features, and elevation.

2.3 Gridded input construction

194   In the previous construction of input features for $PM_{2.5}$ sites, we used location information,
195   time information, meteorological information from 20 surrounding meteorological stations,

196   emission information, and elevation. If we assume that each cell in grid cells is a virtual $PM_{2.5}$ site,
197   then it is possible to generate input features for each grid point. After the model is trained based on
198   input features and $PM_{2.5}$ concentrations at real $PM_{2.5}$ sites, we can feed the gridded input data into
199   the model in turn and consequently construct a gridded $PM_{2.5}$ network. Therefore, we define a grid
200   area at 0.25°×0.25° with longitude from 70°E to 150°E and latitude from 10°N to 60°N and select
201   the grid points covering mainland China. For each grid point, we performed spatiotemporal feature
202   extraction and generated the same 71 input features as those of real $PM_{2.5}$ sites.

2.4 Model description

204   LightGBM is one of the state-of-the-art gradient boosting frameworks with better accuracy,
205   lower memory usage, faster training speed, and capability of handling large-scale data (Ke et al.,
206   2017). Our previous research used this machine learning model to predict $PM_{2.5}$ mass concentrations,
207   which shows an unprecedented predictive capacity on hourly, daily, monthly, and annual
208   timescales(Zhong et al., 2021). This study will continue to use this algorithm and previously tuned
209   hyperparameters for model development (Zhong et al., 2021). For hindcasting historical $PM_{2.5}$
210   datasets prior to 2013, a LightGBM model is trained and validated based on $PM_{2.5}$ observations and
211   feature inputs from 2013 to 2020. The hindcast capability is validated using cross-validation
212   methods, which are standard methods for parameter tuning and model validation in machine
213   learning. The training dataset is divided into several parts, one of them is used as test data, and the
214   remaining are used as training data in turn. Each result yields a corresponding evaluation value,
215   which is then averaged to provide an estimate of the model's accuracy. This estimation is quantified
216   by two metrics, including the coefficient of determination (R^2) and root-mean-square error (RMSE).
217   The hindcast capability is also validated using $PM_{2.5}$ observations from the US embassies in Beijing
218   and Shanghai, which have been observing $PM_{2.5}$ data since as early as 2008. After model training
219   and validation, historical 6-hourly input data are inputted into this model to reconstruct a site-based
220    $PM_{2.5}$ dataset at 6-hour intervals from 1960 to 2020; and gridded input data are inputted into the
221   model to reconstruct a 0.25°×0.25°, 6-hourly, gridded $PM_{2.5}$ dataset. The daily, monthly, yearly, and
222   decadal average $PM_{2.5}$ concentrations for each site and each grid are also calculated based on the
223   two datasets. Monthly-average values were obtained with daily values no less than 20 days;
224   otherwise, they will be missing. Year-average values were calculated with 12 valid month values,
225   and decadal-average values were calculated with 10 valid year-average values. The flowchart of
226   reconstructing $PM_{2.5}$ datasets is shown in Fig. 1.
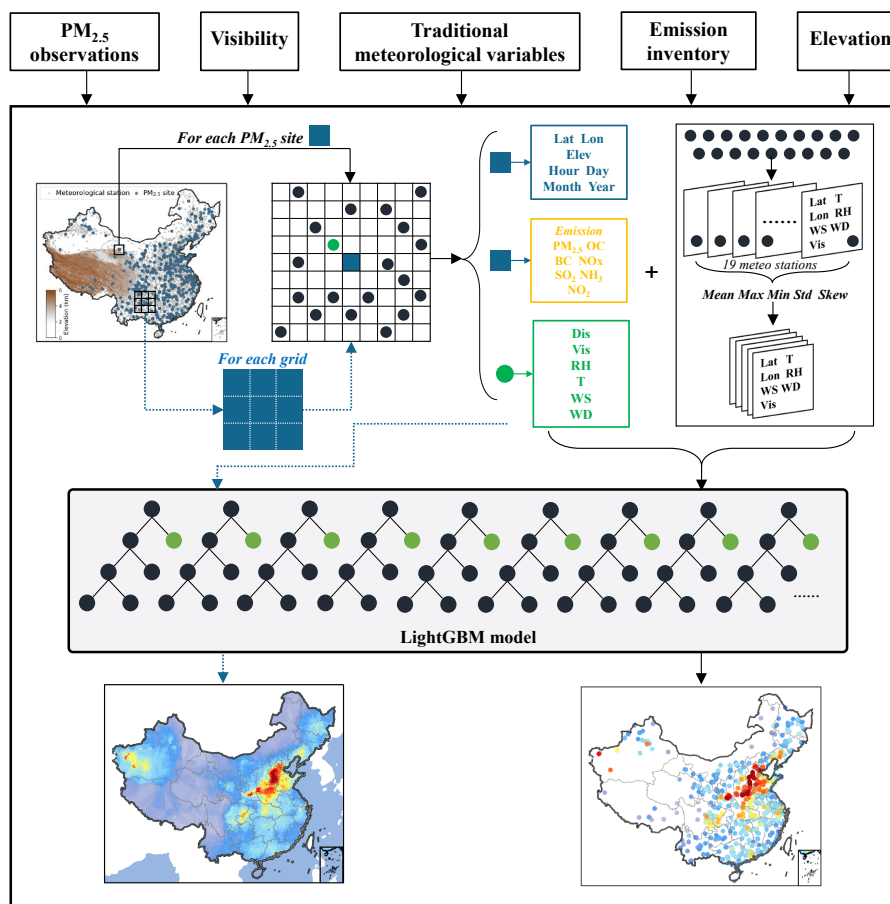
228   **Fig. 1** A conceptual scheme for constructing long-term historical site-based and gridded PM$_{2.5}$
229   records based on long-term visibility, conventional meteorological observations, emissions, and
230   elevation.
231

3 Results and Discussion

3.1 Evaluation of model hindcast performance

The hindcast performance of our model is evaluated using two CV methods, including 10-fold CV and by-year CV. The 10-fold CV partitions the original training datasets into 10 subsamples, one of which is retained as the validation data in turn for testing the model, and the remaining 9 subsamples are used as training data. This method is the most common CV that can be compared with results in other studies. However, 10-fold CV often overestimates the model's ability to hindcast continuous historical data. Therefore, we also use by-year CV, during which one year of data is selected sequentially for testing, and the remaining data are used for model training. This method is specifically designed to evaluate the hindcast capability of the model.

Tab. 1 Model performance in primary predictors, temporal resolution, and hindcast capability compared with other national $PM_{2.5}$ datasets in China.

Related studies	Primary predictors	Temporal resolution	CV type	CV resolution	CV R^2	CV RMSE
Ma et al., 2016	AOD	daily (2004-2013)	10-fold CV	daily	0.79	27.40
			by-year CV		0.41	
Fang et al., 2016	AOD	daily (2013-2014)	10-fold CV	daily	0.80	22.80
Liu et al., 2017	Visibility	monthly (1957-1964, 1973-2014)	10-fold CV	monthly	0.71	25.62
Xiao et al., 2018	AOD	daily (2013-2017)	10-fold CV	daily	0.79	21.00
Xue et al., 2019	AOD、CTM outputs	daily (2000-2016)	by-year CV	daily	0.61	27.80
Liang et al., 2020	AOD	monthly (2000-2016)	10-fold CV	monthly	0.93	6.20
Huang et al., 2021	AOD、CTM outputs	daily (2013-2019)	10-fold CV	daily	0.87-0.88	11.90-21.90
			by-year CV		0.62	27.70
Wei et al, 2021	AOD	monthly (2000-2020)	10-fold CV	monthly	0.86–0.90	10.00-18.40
			by-year CV		0.80	11.26
van Donkelaar et al. 2021	AOD、CTM outputs	monthly (1998-2020)	Non-CV	yearly	0.69	11.90
Geng et al., 2021	AOD、CTM outputs	daily (2000-2020)	out-of-bag CV	daily	0.80-0.88	13.90-22.10
			by-year CV		0.58	27.50
Bai et al., 2022	AOD	daily (2000-2020)	10-fold CV	daily	0.79	20.04
Our study	Visibility	6-hourly (1960-2020)	10-fold CV	hourly/6-hourly	0.79	20.07
				6-hourly	0.78	21.14
				daily	0.85	16.11
				monthly	0.92	7.90
			by-year CV	hourly/6-hourly	0.70	26.36
				6-hourly	0.71	25.63
				daily	0.78	20.90
				monthly	0.83	13.37

Table 1 compares our dataset and the available datasets in primary predictors, temporal resolution, and CV results(Ma et al., 2016; Fang et al., 2016; Liu et al., 2017; Xiao et al., 2018; Xue et al., 2019; Liang et al., 2020; Huang et al., 2021; Wei et al., 2021; Van Donkelaar et al., 2021; Geng et al., 2021; Bai et al., 2022). AOD-based datasets are only available from around 2000 at the earliest, with temporal resolutions ranging from daily scale to monthly scale. In contrast, our visibility-based dataset spans 61 years from 1960 to 2020 at 6-hourly intervals, showing a clear advantage in terms of time span and resolution. The R^2 and RMSE values of our 10-fold CV results are 0.78 and 21.14 μg m^{-3} for 6-hourly estimations, respectively, which indicates our model is quite robust in estimating $PM_{2.5}$. Due to a reduction in data amount, the R^2 and RMSE values further improved to 0.85 and 16.11 μg m^{-3} for daily estimations and 0.92 and 7.90 μg m^{-3} for monthly estimations. This result is comparable or even better than those of other available datasets whose 10-fold CV R^2 ranges from 0.61 to 0.80 for daily scale and from 0.71 to 0.93 for monthly scale. Our by-year CV's R^2 and RMSE values are 0.71 and 25.63 μg m^{-3} for 6-hourly estimations, which indicates our model is still robust in hindcast performance. The by-year CV R^2 values for daily and monthly estimations (0.78 and 0.83) are higher than those in other available datasets (0.41-0.62 and

260   0.80), which might be partly attributed to spatial feature extraction and the large volume of our
261   training dataset. Zhong et al. (2021) has shown that extracting spatial features can result in a better
262   hindcast performance by fully representing dimensional heterogeneity. Compared to hundreds of
263   thousands to millions of training samples in AOD-based models, the training samples for the
264   visibility-based model are over 100 million. An increase in the order of magnitude for training
265   datasets will yield better results in machine learning.
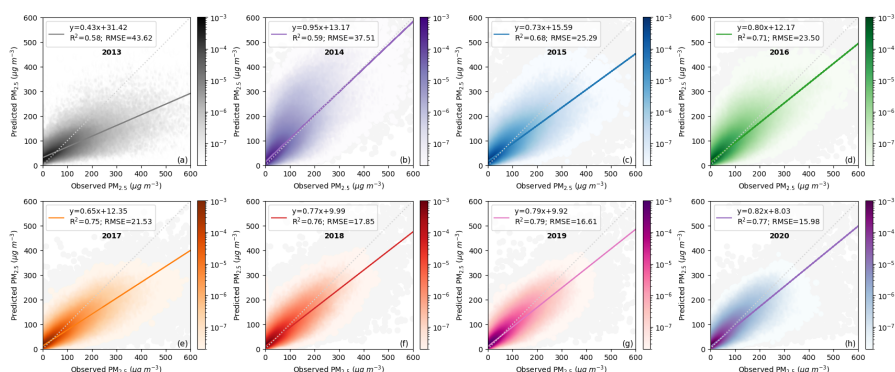
267   **Fig. 2** Density scatterplots of observed PM$_{2.5}$ and estimated PM$_{2.5}$ across China for by-year CV
268   from 2013 to 2020 (Colors are probability distribution densities).

269

270   The refined by-year CV results for each year between 2013-2020 are shown in Fig. 2. The
271   by-year CV R^2 lies between 0.58 and 0.79, with better hindcast performance after 2014. The
272   potential reasons why the R^2 value in 2013 is slightly lower than those in other years are as follows.
273   First, the PM$_{2.5}$ observation network was just established in 2013, during which dehumidification
274   systems, processing procedures, and data quality control methods are incomplete, and therefore the
275   overall data quality cannot be guaranteed. With the improvement of the observation network after
276   2014, both the quality and quantity of observations increase significantly. This situation where data
277   quality is relatively low initially but increased over time is also found in O$_3$ observations. Second,
278   the CMA began to convert some of the manual visibility observations to automatic observations in
279   2013, during which there were also some irregular procedures in instrument equipment, observation
280   steps, and data quality control. Lastly, although we have corrected the biases between manual and
281   automated observations, some biases may still exist. However, the biases are further reduced as we
282   integrate all manual visibility observations in 2013 into our training dataset.
283   The model's hindcast capability is further evaluated independently using pre-2013 PM$_{2.5}$
284   observations. For the PM$_{2.5}$ data currently available, only the US embassies in Beijing and Shanghai
285   have at least one year's PM$_{2.5}$ observations. Therefore, PM$_{2.5}$ data from these two sites are applied
286   as an independent evaluation dataset. Figure 3 shows our estimated PM$_{2.5}$ are in close agreement
287   with in-situ measurements in Beijing and Shanghai, where the overall R^2 between observations and
288   estimations is 0.74 and 0.79, respectively. For each year between 2008-2012 in Beijing, the R^2
289   values fluctuated between 0.70 and 0.81, reflecting a stable and accurate by-year hindcast capability.
290   As shown in Fig. 3 (c-h), the low values, high values, and temporal variations in PM$_{2.5}$
291   measurements are all well estimated. In particular, PM$_{2.5}$ measurements are lacking at the US
292   Embassy in Beijing in early 2008 and around 2009, but our model can provide reasonable and

293 continuous estimations to fill in the gaps. This ability can also be used to fill in missing PM$_{2.5}$
294 observations of MEE from 2013 onwards, building a complete PM$_{2.5}$ dataset. Overall, the
295 independent validation results show that historical PM$_{2.5}$ data can be well reconstructed by our
296 model.
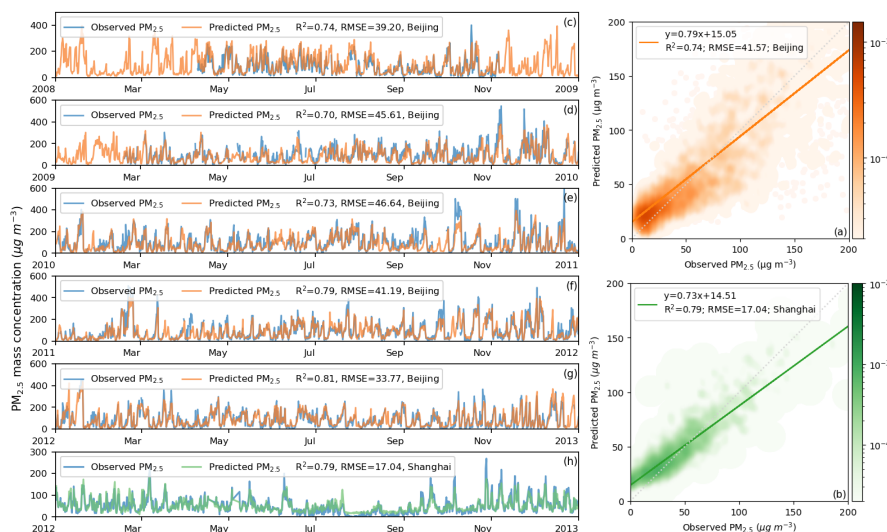
298 **Fig. 3** (a) Density scatterplots of observed PM$_{2.5}$ and estimated PM$_{2.5}$ between 2008-2012 at the
299 US Embassy in Beijing; (b) Density scatterplots of observed PM$_{2.5}$ and estimated PM$_{2.5}$ in 2012 at
300 the US Embassy in Shanghai; (c-g) Timeseries of observed PM$_{2.5}$ and estimated PM$_{2.5}$ for each
301 year between 2008-2012 at the US Embassy in Beijing; and (h) Timeseries of observed PM$_{2.5}$ and
302 estimated PM$_{2.5}$ for each year in 2012 at the US Embassy in Shanghai.

303 **3.2 Spatiotemporal variations in the site-based PM$_{2.5}$ dataset during 1960-2020**

304 Figure 4 shows the spatiotemporal variations in annual average site-based PM$_{2.5}$ between 1960-
305 2020. The trend of PM$_{2.5}$ in China experiences three major stages, corresponding to a slow increase
306 under low concentrations between 1960-1978, a continuous accumulation with high concentrations
307 reached between 1979-2013, and a rapid decrease between 2014-2020. During the first stage, though
308 PM$_{2.5}$ pollution occurred in parts of the NCP and the Guanzhong Plain (GZP), PM$_{2.5}$ concentrations
309 remain low in the vast majority of areas. This is mainly because anthropogenic emissions of PM$_{2.5}$
310 precursors and primary PM$_{2.5}$ grow slowly at a low base, resulting in relatively low total emissions
311 in different regions. However, PM$_{2.5}$ pollution still occurring in the NCP and GZP, even with
312 relatively low emissions, indicates the low environmental capacity of these two regions. During the
313 second stage, PM$_{2.5}$ reached an unprecedentedly high concentration after a continuous increase in
314 nearly all regions in China. The heaviest PM$_{2.5}$ pollution occurred in the NCP and the GZP. The SB
315 and the Northeast China Plain (NeCP) are the polluted regions with the next highest PM$_{2.5}$ pollution.
316 Even the YRD and the PRD also experienced PM$_{2.5}$ pollution during this stage. This worsening of
317 PM$_{2.5}$ pollution is closely associated with massive anthropogenic emissions from rapidly increasing
318 living and industrial activities after reform and opening-up policies. From 1979 to 2013, primary
319 PM$_{2.5}$, NOx, SO$_2$, NH$_3$, BC, OC, and CO from the Peking emission inventory increased by 98%,

320   457%, 159%, 117%, 45%, -22%, and 243%, respectively. Despite a slow reduction in SO_2 after
321   2006, the total anthropogenic emissions each year still increase and thereby cause high-level $PM_{2.5}$
322   pollution after 2006. The results indicate that air pollutants cannot be emitted without restraint, even
323   in regions with high atmospheric capacity. Otherwise, $PM_{2.5}$ pollution will inevitably occur. In
324   addition to anthropogenic emissions, sand and dust storms, resulting in high $PM_{2.5}$ concentrations
325   in western Xinjiang, worsened $PM_{2.5}$ pollution by trans-regional transport from the desert regions.
326   During the last stage, $PM_{2.5}$ decreased nationwide with the mass concentrations in nearly all stations
327   approximately or below 35 ug m^{-3} in 2020, even in the NCP and the GZP with limited environmental
328   capacity. The substantial declines in $PM_{2.5}$ illustrate the effectiveness of implementing the toughest-
329   ever clean air policy in China. The spatiotemporal variations of $PM_{2.5}$ between 1960-2020 clearly
330   show the long-term impact of economic development and energy consumption on our air quality
331   and the effectiveness of recent years' unprecedented emission control policies.
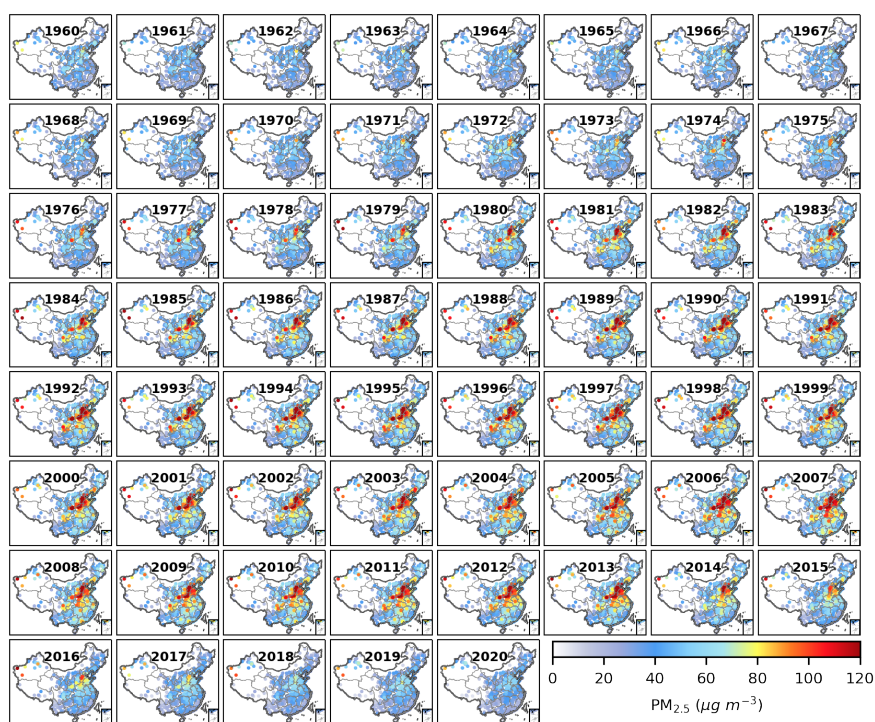
333   **Fig. 4** Spatial distribution of annual average $PM_{2.5}$ mass concentration at 1485 stations from 1960
334   to 2020
335
336   The specific turning points in annual $PM_{2.5}$ concentrations for different regions were
337   investigated additionally. Figure 5 shows the temporal variations in national-average monthly and
338   yearly $PM_{2.5}$ mass concentrations and regional average 6-hourly, monthly, and yearly $PM_{2.5}$ mass
339   concentrations in "2+26" cities of the NCP, the YRD, the PRD, and the SB. The national-average
340   yearly $PM_{2.5}$ reached a peak of 67 ug m^{-3} in 2007, declined in 2008, and then remained steady until
341   2013. A sharp fall followed after 2014 with $PM_{2.5}$ concentrations decreasing from 63 ug m^{-3} in 2013

Earth System
Science
Data

to 34 ug m^{-3} in 2020. The annual PM$_{2.5}$ concentrations in the "2+26" cities also experienced similar
changes with a peak at 2007 and a reduction in 2008, which might be related to emission reduction
for the Beijing Olympics in 2008. For the YRD, the maximum value of PM$_{2.5}$ mass concentration
occurred in 2013 without a striking peak in 2007. For the PRD, the annual PM$_{2.5}$ concentrations
increased steadily between 1960-1978, then rose more and more steeply in the following years with
a steep increase in 2003 and 2004 and peaked in 2004. A steady decrease with slight fluctuation
occurred in 2005-2013, and then a sharp fall followed after 2014. This trend is different from that
in the "2+26" cities and the YRD. For the SB, the turning point occurred in 2013, before which the
annual PM$_{2.5}$ concentrations increased steadily and remained steady.
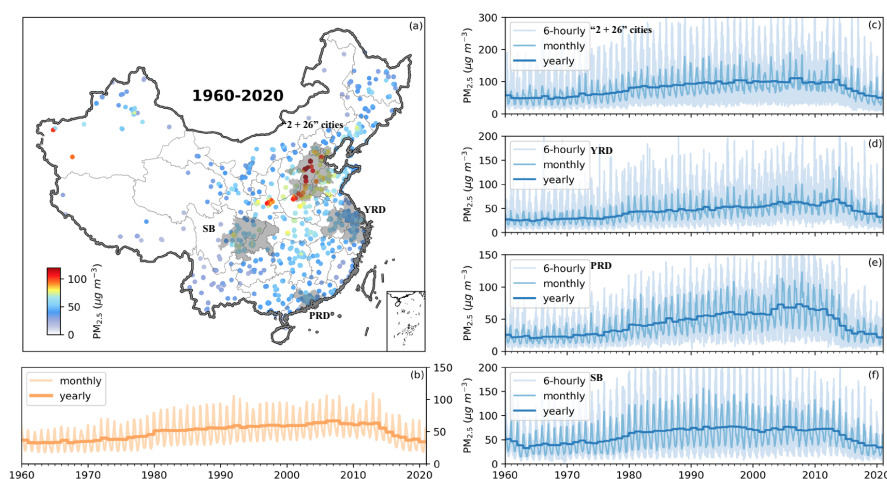
Fig. 5 (a) Spatial distribution of average PM$_{2.5}$ mass concentrations between 1960-2020; (b-f)
Timeseries of average PM$_{2.5}$ mass concentrations for all sites in China (b), "2+26" cities (c),
Yangtze River Delta (d), Pearl River Delta (e) and Sichuan Basin (f), respectively.

3.3 Detailed spatial distributions from gridded PM$_{2.5}$ datasets

The model's ability to make PM$_{2.5}$ predictions at locations outside the scope of the training
stations is evaluated by spatial CV. For spatial CV, all the monitoring stations are randomly divided
into five subsets, and the model is trained using data from four subsets and tested on the data from
the remaining subset each time. As shown in Fig. 6, the R^2 for spatial cross-validation in different
groups is between 0.75 and 0.79, reflecting robust predictive power for PM$_{2.5}$ concentrations at sites
outside the training sites. Our previous study also examined this predictive ability using PM$_{2.5}$ data
from 23 untouched regional PM$_{2.5}$ stations (Zhong et al., 2021).
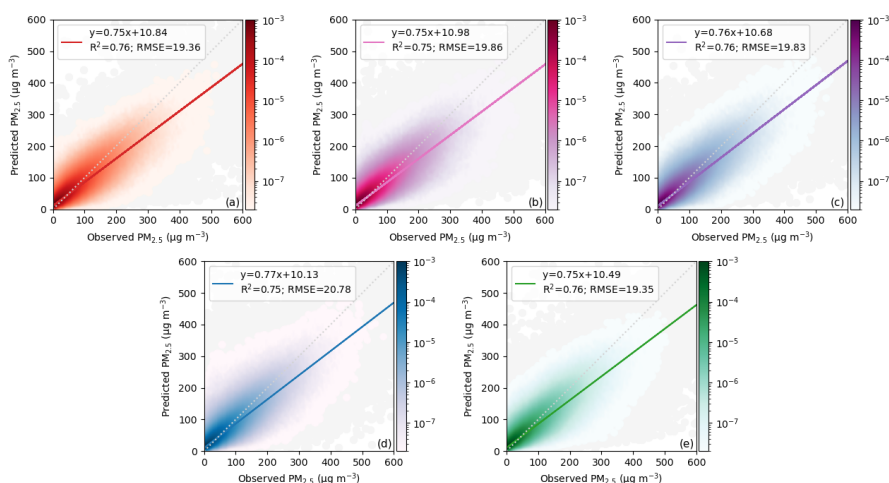
Fig. 6 Density scatterplots of observed $PM_{2.5}$ and estimated $PM_{2.5}$ for each group of spatial CV results

Figure 7 shows the annual spatial variations in 0.25°×0.25° gridded $PM_{2.5}$ between 1960-2020. Compared to site-based distributions, gridded $PM_{2.5}$ can portray the spatiotemporal variations in a clearer and more detailed way. For example, the most widespread and heaviest $PM_{2.5}$ pollution in western Xinjiang occurred in 1979. This abnormal pollution corresponds to the historical construction of northern severe dust storms, which recorded the event with the largest affected areas in April 1979 (Zhou and Zhang, 2003). As exposed to nearly the most frequent air stagnation in winter due to terrain and meteorological conditions (Wang et al., 2018), the NCP is the region with $PM_{2.5}$ pollution first to appear and last to disappear except areas affected by dust storms (Fig. 7). For year-to-year comparisons, it can be clearly seen that $PM_{2.5}$ concentrations in the NCP decreased slightly from 2007 to 2008 and from 2012 to 2013, respectively, and decreased significantly in 2014 relative to 2013. The $PM_{2.5}$ reduction is insignificant from 2015 to 2016 but striking from 2016 to 2017. In 2020, the nationwide $PM_{2.5}$ concentrations are comparable to those in 1960s and close to the lowest level ever recorded in almost 61 years.
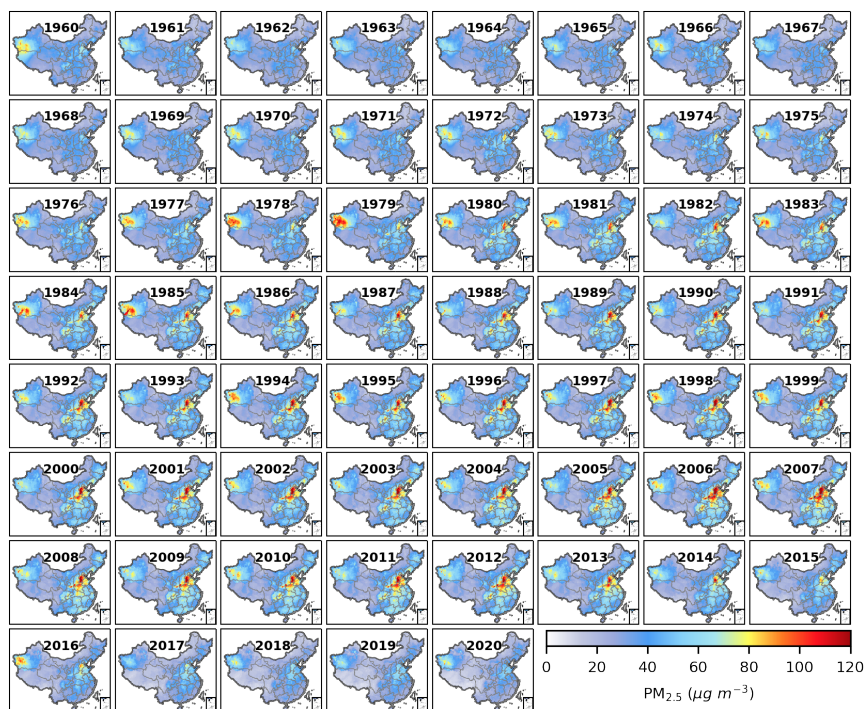
381 **Fig. 7** Gridded distribution of annual average PM$_{2.5}$ mass concentration from 1960 to 2020

382

383   Figure 8 shows inter-decadal spatial variations in gridded PM$_{2.5}$ between 1961-2020. PM$_{2.5}$

384 concentrations maintained at low levels in most areas over the first decade and increased to a certain

385 extent in the NCP and western Xinjiang over the second decade. In the following decades, PM$_{2.5}$

386 pollution has worsened significantly in several key regions, including the NCP, the GZP, and the SB.

387 This worsening is maintained until the last decade, during which PM$_{2.5}$ pollution mitigates

388 significantly in nearly all populous and polluted regions in eastern China.
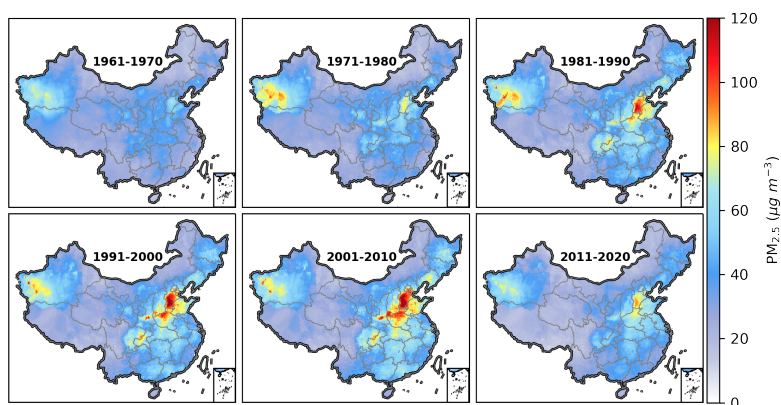
390 **Fig. 8** Gridded distribution of decadal average PM$_{2.5}$ mass concentration from 1960 to 2020

391   The multi-year trend of our gridded PM$_{2.5}$ dataset is also compared with those of publicly
392   available datasets, including the TAP data (Geng et al., 2021), the GEFPM data (Van Donkelaar et
393   al., 2021), the LGHAP data (Bai et al., 2022), and the CHAP data (Wei et al., 2021), which have
394   been interpolated to the same grid resolution. Figure 9 shows the spatial distributions of PM$_{2.5}$ from
395   those datasets at 5-year intervals between 2000-2020. One consistent trend across all datasets was
396   that nationwide PM$_{2.5}$ mass concentrations experienced an increase following a decrease from 2000
397   to 2020. However, the turning points are different for different datasets. From 2010 to 2015, PM$_{2.5}$
398   pollution alleviated for TAP, CHAP, and our data but worsened for GEFPM and LGHAP. For the
399   time (2015 and 2020) with ground observations available, all PM$_{2.5}$ data show similar spatial
400   distributions with the most severe pollution in the NCP in 2015 and significant improvement in
401   nationwide air pollution in 2020. For the years (2000, 2005, and 2010) when ground observations
402   were unavailable, significant disparities in pollution levels and regional distribution emerged from
403   different datasets. Specifically, the LGHAP data are significantly lower than other data, while the
404   TAP data are higher than others in nearly all regions except western Xinjiang. In western Xinjiang,
405   PM$_{2.5}$ concentrations from the GEFPM data are the highest among all the datasets. Due to a lack of
406   ground PM$_{2.5}$ observations before 2000, it's challenging to determine which dataset has the least
407   bias and more reasonable distributions. In the future, applying ensemble average to multi-datasets
408   might be an effective way to eliminate systematic bias.
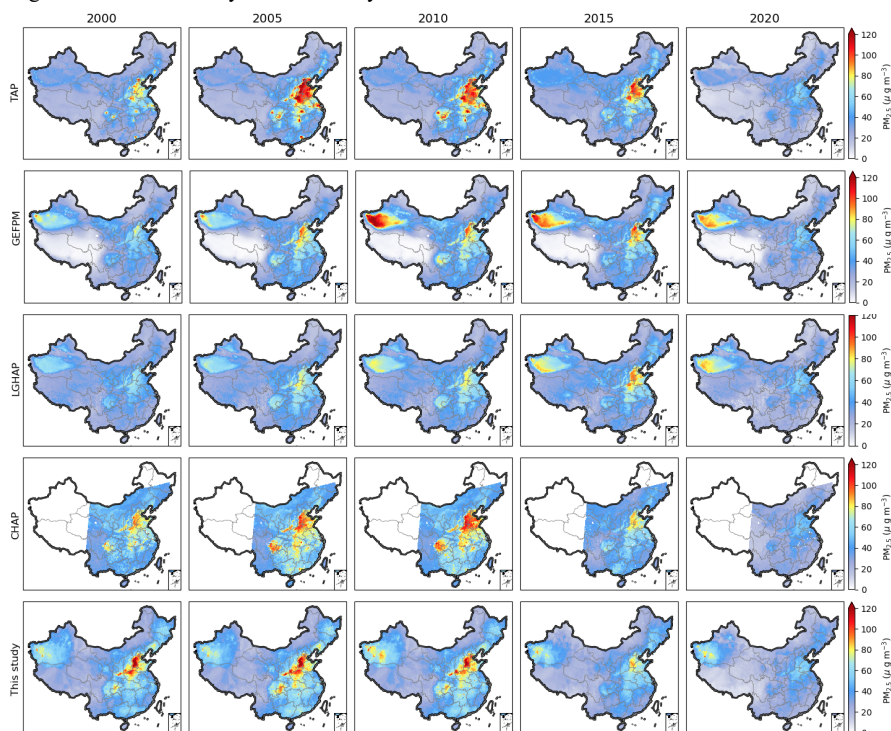
410   **Fig. 9** Distribution of reconstructed PM$_{2.5}$ by different PM$_{2.5}$ datasets in 2000, 2005, 2010, 2015,
411   and 2020. From top to down are TAP, GEFPM, LGHAP, CHAP, and our dataset.
412

4 Data availability

The 6-hourly $PM_{2.5}$ datasets from 1960 to 2020, including site-based and gridded data, are publicly accessible. Daily, monthly, and yearly sited-based and gridded $PM_{2.5}$ datasets are also provided. The sited-based $PM_{2.5}$ dataset are in the CSV format, and the gridded dataset $PM_{2.5}$ are in the NETCDF format. All of them are available at https://doi.org/10.5281/zenodo.6372847 (Zhong et al., 2022).

5 Conclusion

This study is among the first to generate long-term site-based and gridded $PM_{2.5}$ datasets between 1960-2020 with 6-hourly resolution, based on long-term visibility, conventional meteorological observations, emissions, and elevation. A new feature engineering method that takes advantage of spatial features from 20 surrounding meteorological stations is employed in our LightGBM model to incorporate spatial effects of meteorological conditions. For by-year CV, The R^2 values of our model are 0.71, 0.78, and 0.83 for 6-hourly, daily, and monthly estimations, respectively, which are higher than those in other available datasets (0.41-0.62). This hindcast capability is further evaluated independently using pre-2013 $PM_{2.5}$ data of 6 years from US embassies in Beijing and Shanghai. The low values, high values, and temporal variations in US-embassy $PM_{2.5}$ measurements are all well estimated with the overall R^2 being 0.74 and 0.79 in Beijing and Shanghai, respectively. Both by-year CV and independent validation show that our model has a stable by-year hindcast capability and can reconstruct historical $PM_{2.5}$ data in a relatively accurate way. Our datasets show that $PM_{2.5}$ variations in China experience a slow increase under low concentrations between 1960-1978, a continuous accumulation with high concentrations reached between 1979-2013, and a rapid decrease between 2014-2020. The worsening of $PM_{2.5}$ pollution is closely associated with massive anthropogenic emissions after reform and opening-up policies, while the substantial declines in $PM_{2.5}$ are mainly due to the implementation of the toughest-ever clean air policy in China. In 2020, the nationwide $PM_{2.5}$ concentrations were close to the lowest recorded level in almost 61 years. These two reconstructed $PM_{2.5}$ datasets provide spatiotemporal variations at high resolution, which lay the foundation of research studies associated with air pollution, climate change, and atmospheric chemical reanalysis. It is worth noting that our datasets still have some weaknesses, with the main weakness being a lack of detailed bias estimations for each value in our datasets due to limited historical observations. In the future, we will collect as many $PM_{2.5}$ observations as possible to validate the accuracy of our datasets and provide evaluations of uncertainty for our datasets.

Acknowledgements

The authors are grateful to all the organization and groups that provided indispensable datasets that we used in this study. We would like to acknowledge to CMA for providing the long-term visibility and MEE for the observational $PM_{2.5}$ data. Also, we acknowledge the MEIC team and Peking for providing the emission inventories and GDEM data provider.

Financial support

This research was supported by the Major Project from Natural Science Foundation of China (42090030).

Author Contributions

XZ designed the research and led the overall scientific questions. JZ, KG, and LG carried out data processing and analysis based on suggestions from ZZ, DW, YW, and HC. LL calibrated $PM_{2.5}$ data and meteorological observations. YF performed visibility conversions from class values to numeric values before 1980. LJ and LJ provided calibrated visibility from 2013 to 2016 and suggestions about manuscript structures. JZ wrote the first draft of the manuscript, and XZ revised the manuscript. All authors read and approved the final version.

Competing financial interests

The authors declare no competing financial interests.

References

Bai, K., Li, K., Ma, M., Li, K., Li, Z., Guo, J., Chang, N. B., Tan, Z., and Han, D.: LGHAP: the Long-term Gap-free High-resolution Air Pollutant concentration dataset, derived via tensor-flow-based multimodal data fusion, Earth Syst. Sci. Data, 14, 907-927, 10.5194/essd-14-907-2022, 2022.

Beelen, R., Hoek, G., Den Brandt, P. A. V., Goldbohm, R. A., Fischer, P., Schouten, L. J., Jerrett, M., Hughes, E., Armstrong, B., and Brunekreef, B.: Long-term effects of traffic-related air pollution on mortality in a Dutch cohort (NLCS-AIR study), Environmental Health Perspectives, 116, 196-202, 2007.

Chen, H., Huang, Y., Shen, H., Chen, Y., Ru, M., Chen, Y., Lin, N., Su, S., Zhuo, S., Zhong, Q., Wang, X., Liu, J., Li, B., and Tao, S.: Modeling temporal variations in global residential energy consumption and pollutant emissions, Applied Energy, 184, 820-829, https://doi.org/10.1016/j.apenergy.2015.10.185, 2016a.

Chen, X., Zhang, L. W., Huang, J. J., Song, F. J., Zhang, L. P., Qian, Z. M., Trevathan, E., Mao, H. J., Han, B., Vaughn, M., Chen, K. X., Liu, Y. M., Chen, J., Zhao, B. X., Jiang, G. H., Gu, Q., Bai, Z. P., Dong, G. H., and Tang, N. J.: Long-term exposure to urban air pollution and lung cancer mortality: A 12-year cohort study in Northern China, Science of the Total Environment, 571, 855-861, 10.1016/j.scitotenv.2016.07.064, 2016b.

CMA: Forecasting and Networking Department of China Meteorological Administration released letter No.4: Notice on the adjustments of the haze weather phenomenon observation and on the revision of the fog and haze observation data, 2014.

Fang, X., Zou, B., Liu, X., Sternberg, T., and Zhai, L.: Satellite-based ground PM2.5 estimation using timely structure adaptive modeling, Remote Sensing of Environment, 186, 152-163, https://doi.org/10.1016/j.rse.2016.08.027, 2016.

Gelaro, R., McCarty, W., Suárez, M. J., Todling, R., Molod, A., Takacs, L., Randles, C. A., Darmenov, A., Bosilovich, M. G., and Reichle, R.: The modern-era retrospective analysis for research and applications, version 2 (MERRA-2), Journal of Climate, 30, 5419-5454, 2017.

Geng, G., Xiao, Q., Liu, S., Liu, X., Cheng, J., Zheng, Y., Xue, T., Tong, D., Zheng, B., Peng, Y., Huang, X., He, K., and Zhang, Q.: Tracking Air Pollution in China: Near Real-Time PM2.5 Retrievals from Multisource Data Fusion, Environmental Science & Technology, 55, 12106-12115, 10.1021/acs.est.1c01863, 2021.

Gui, K., Che, H., Zeng, Z., Wang, Y., Zhai, S., Wang, Z., Luo, M., Zhang, L., Liao, T., Zhao, H., Li, L., Zheng, Y., and Zhang, X.: Construction of a virtual PM2.5 observation network in China based on high-density surface meteorological observations using the Extreme Gradient Boosting model, Environment International, 141, 105801, https://doi.org/10.1016/j.envint.2020.105801, 2020.

Huang, C., Hu, J., Xue, T., Xu, H., and Wang, M.: High-Resolution Spatiotemporal Modeling for Ambient PM2.5 Exposure Assessment in China from 2013 to 2019, Environmental Science & Technology, 55, 2152-2162, 10.1021/acs.est.0c05815, 2021.

Huang, Y., Shen, H., Chen, Y., Zhong, Q., Chen, H., Wang, R., Shen, G., Liu, J., Li, B., and Tao, S.: Global organic carbon emissions from primary sources from 1960 to 2009, Atmospheric Environment, 122, 505-512, https://doi.org/10.1016/j.atmosenv.2015.10.017, 2015.

Huang, Y., Shen, H., Chen, H., Wang, R., Zhang, Y., Su, S., Chen, Y., Lin, N., Zhuo, S., Zhong, Q., Wang, X., Liu, J., Li, B., Liu, W., and Tao, S.: Quantification of Global Primary Emissions of PM2.5, PM10, and TSP from Combustion and Industrial Process Sources, Environmental Science & Technology,

508   48, 13834-13843, 10.1021/es503696k, 2014.

509   Inness, A., Ades, M., Agustí-Panareda, A., Barré, J., Benedictow, A., Blechschmidt, A. M., Dominguez,
510   J. J., Engelen, R., Eskes, H., Flemming, J., Huijnen, V., Jones, L., Kipling, Z., Massart, S., Parrington,
511   M., Peuch, V. H., Razinger, M., Remy, S., Schulz, M., and Suttie, M.: The CAMS reanalysis of
512   atmospheric composition, Atmos. Chem. Phys., 19, 3515-3556, 10.5194/acp-19-3515-2019, 2019.

513   Ke, G., Meng, Q., Finley, T., Wang, T., Chen, W., Ma, W., Ye, Q., and Liu, T.-Y.: Lightgbm: A highly
514   efficient gradient boosting decision tree, Advances in neural information processing systems, 3146-
515   3154,

516   Liang, F., Xiao, Q., Huang, K., Yang, X., Liu, F., Li, J., Lu, X., Liu, Y., and Gu, D.: The 17-y
517   spatiotemporal trend of PM$_{2.5}$ and its mortality burden in China, Proceedings of the
518   National Academy of Sciences, 117, 25601-25608, 10.1073/pnas.1919641117, 2020.

519   Liu, M., Bi, J., and Ma, Z.: Visibility-Based PM2.5 Concentrations in China: 1957–1964 and 1973–2014,
520   Environmental Science & Technology, 51, 13161-13169, 10.1021/acs.est.7b03468, 2017.

521   Lynch, P., Reid, J. S., Westphal, D. L., Zhang, J., Hogan, T. F., Hyer, E. J., Curtis, C. A., Hegg, D. A.,
522   Shi, Y., and Campbell, J. R.: An 11-year global gridded aerosol optical thickness reanalysis (v1. 0)
523   for atmospheric and climate sciences, Geoscientific Model Development, 9, 1489, 2016.

524   Ma, Z., Hu, X., Sayer, A. M., Levy, R., Zhang, Q., Xue, Y., Tong, S., Bi, J., Huang, L., and Liu, Y.:
525   Satellite-Based Spatiotemporal Trends in PM2.5 Concentrations: China, 2004-2013, Environmental
526   Health Perspectives, 124, 184-192, doi:10.1289/ehp.1409481, 2016.

527   Pope, C. A., Burnett, R. T., Thun, M. J., Calle, E. E., Krewski, D., Ito, K., and Thurston, G. D.: Lung
528   cancer, cardiopulmonary mortality, and long-term exposure to fine particulate air pollution, Journal
529   of the American Medical Association, 287, 1132-1141, 2002.

530   Randles, C., Da Silva, A., Buchard, V., Colarco, P., Darmenov, A., Govindaraju, R., Smirnov, A., Holben,
531   B., Ferrare, R., and Hair, J.: The MERRA-2 aerosol reanalysis, 1980 onward. Part I: System
532   description and data assimilation evaluation, Journal of Climate, 30, 6823-6850, 2017.

533   van Donkelaar, A., Hammer, M. S., Bindle, L., Brauer, M., Brook, J. R., Garay, M. J., Hsu, N. C.,
534   Kalashnikova, O. V., Kahn, R. A., Lee, C., Levy, R. C., Lyapustin, A., Sayer, A. M., and Martin, R.
535   V.: Monthly Global Estimates of Fine Particulate Matter and Their Uncertainty, Environmental
536   Science & Technology, 10.1021/acs.est.1c05309, 2021.

537   Wang, R., Tao, S., Shen, H., Huang, Y., Chen, H., Balkanski, Y., Boucher, O., Ciais, P., Shen, G., Li, W.,
538   Zhang, Y., Chen, Y., Lin, N., Su, S., Li, B., Liu, J., and Liu, W.: Trend in Global Black Carbon
539   Emissions from 1960 to 2007, Environmental Science & Technology, 48, 6780-6787,
540   10.1021/es5021422, 2014.

541   Wang, X., Dickinson, R. E., Su, L., Zhou, C., and Wang, K.: PM 2.5 Pollution in China and How It Has
542   Been Exacerbated by Terrain and Meteorological Conditions, Bulletin of the American
543   Meteorological Society, 99, 105-119, 10.1175/bams-d-16-0301.1, 2018.

544   Wei, J., Li, Z., Lyapustin, A., Sun, L., Peng, Y., Xue, W., Su, T., and Cribb, M.: Reconstructing 1-km-
545   resolution high-quality PM2.5 data records from 2000 to 2018 in China: spatiotemporal variations
546   and policy implications, Remote Sensing of Environment, 252, 112136,
547   https://doi.org/10.1016/j.rse.2020.112136, 2021.

548   Xiao, Q., Chang, H. H., Geng, G., and Liu, Y.: An Ensemble Machine-Learning Model To Predict
549   Historical PM2.5 Concentrations in China from Satellite Data, Environmental Science &
550   Technology, 52, 13260-13269, 10.1021/acs.est.8b02917, 2018.

551   Xue, T., Zheng, Y., Tong, D., Zheng, B., Li, X., Zhu, T., and Zhang, Q.: Spatiotemporal continuous

552   estimates of PM2.5 concentrations in China, 2000–2016: A machine learning method with inputs
553   from satellites, chemical transport model, and ground observations, Environment International, 123,
554   345-357, https://doi.org/10.1016/j.envint.2018.11.075, 2019.

555   Yumimoto, K., Tanaka, T. Y., Oshima, N., and Maki, T.: JRAero: the Japanese reanalysis for aerosol v1.
556   0, Geoscientific Model Development, 10, 3225, 2017.

557   Zhang, Q., Streets, D. G., Carmichael, G. R., He, K., Huo, H., Kannari, A., Klimont, Z., Park, I., Reddy,
558   S., and Fu, J.: Asian emissions in 2006 for the NASA INTEX-B mission, Atmospheric Chemistry
559   and Physics, 9, 5131-5153, 2009.

560   Zheng, B., Cheng, J., Geng, G., Wang, X., Li, M., Shi, Q., Qi, J., Lei, Y., Zhang, Q., and He, K.: Mapping
561   anthropogenic emissions in China at 1 km spatial resolution and its application in air quality
562   modeling, Science Bulletin, 66, 612-620, https://doi.org/10.1016/j.scib.2020.12.008, 2021.

563   Zheng, B., Tong, D., Li, M., Liu, F., Hong, C., Geng, G., Li, H., Li, X., Peng, L., Qi, J., Yan, L., Zhang,
564   Y., Zhao, H., Zheng, Y., He, K., and Zhang, Q.: Trends in China's anthropogenic emissions since
565   2010 as the consequence of clean air actions, Atmos. Chem. Phys., 18, 14095-14111, 10.5194/acp-
566   18-14095-2018, 2018.

567   Zhong, J., Zhang, X., Dong, Y., Wang, Y., Liu, C., Wang, J., Zhang, Y., and Che, H.: Feedback effects of
568   boundary-layer meteorological factors on cumulative explosive growth of PM2.5 during winter
569   heavy pollution episodes in Beijing from 2013 to 2016, Atmos. Chem. Phys., 18, 247-258,
570   10.5194/acp-18-247-2018, 2018.

571   Zhong, J., Zhang, X., Gui, K., Wang, Y., Che, H., Shen, X., Zhang, L., Zhang, Y., Sun, J., and Zhang, W.:
572   Robust prediction of hourly PM2.5 from meteorological data using LightGBM, National Science
573   Review, 8, 10.1093/nsr/nwaa307, 2021.

574   Zhong, J., Zhang, X., Wang, Y., Sun, J., Zhang, Y., Wang, J., Tan, K., Shen, X., Che, H., and Zhang, L.:
575   Relative contributions of boundary-layer meteorological factors to the explosive growth of PM2.5
576   during the red-alert heavy pollution episodes in Beijing in December 2016, Journal of
577   Meteorological Research, 31, 809-819, 10.1007/s13351-017-7088-0, 2017.

578   Zhong, J., Zhang, X., Gui, K., Liao, J., Fei, Y., Jiang, L., Guo, L., Liu, L., Che, H., Wang, Y., Wang, D.,
579   and Zhou, Z.: Reconstructing 6-hourly PM2.5 datasets from 1960 to 2020 in China [dataset],
580   10.5281/zenodo.6372847, 2022.

581   Zhou, Z. and Zhang, G.: Typical severe dust storms in northern China during 1954—2002, Chinese
582   Science Bulletin, 48, 2366-2370, 2003.

583

584